

Ab Initio Theory of Large Phonon Magnetic Moments Induced by Electron-Phonon Coupling in Magnetic Materials

Fuyi Wang¹, Xinqi Liu¹, Hong Sun², Huaqiang Wang^{2,*}, Shuichi Murakami³, Lifa Zhang², Haijun Zhang^{1,4,5,*} and Dingyu Xing^{1,4,5}

¹ National Laboratory of Solid State Microstructures,

School of Physics, Nanjing University, Nanjing 210093, China

² Center for Quantum Transport and Thermal Energy Science,

School of Physics and Technology, Nanjing Normal University, Nanjing 210023, China

³ Department of Physics, Tokyo Institute of Technology,

2-12-1 Ookayama, Meguro-ku, Tokyo 152-8551, Japan

⁴ Collaborative Innovation Center of Advanced Microstructures, Nanjing University, Nanjing 210093, China

⁵ Jiangsu Physical Science Research Center, Nanjing 210093, China*

(Dated: April 10, 2025)

Chiral phonons, characterized by nonzero angular momenta and magnetic moments, have attracted extensive attention. However, a long-standing critical issue in this field is the lack of an approach to accurately calculate phonon magnetic moments resulting from electron-phonon coupling (EPC) in realistic materials. Here, based on the linear response framework, we develop an *ab initio* theory for calculating EPC-induced magnetic properties of phonons, applicable to both insulating and metallic materials. Then, we evidently demonstrate EPC-induced large phonon magnetic moments and phonon Zeeman splittings resulting from spin-phonon coupling in magnetic metals. Interestingly, these splittings can open substantial topologically nontrivial phonon gaps, generating intrinsic phonon Chern states. Further, by constructing an inertially decoupled lattice model, we predict candidate materials exhibiting such intrinsic phonon Chern states with robust edge phonon currents which are proposed to detect neutral particles, such as dark matter particles. Our work enables *ab initio* calculations for EPC-induced magnetic properties of phonons and long-sought magnetic phonon spectra.

Introduction. Chiral phonons, collective vibrations stemming from the circular motion of atoms in solids with nonzero angular momentum, were initially proposed by Zhang and Niu [1, 2] and subsequently verified experimentally in monolayer WSe₂ [3]. Recently, there has been a surge of research interest in chiral phonons, covering both theoretical investigations [4–18] and experiments [19–27]. Of particular importance are phonon magnetic moments (PMMs) and phonon Zeeman splittings, which play a crucial role in chiral-phonon-involved effects, such as ultrafast Einstein-de Haas Effect [20] and Barnett effect [22, 28]. However, classical models based on point-charge approximations yield PMM values that are orders of magnitude below experimental measurements [11, 19]. While electron-phonon coupling (EPC) has been indicated as a promising route to enhance PMMs [8, 11, 15], an *ab initio* approach capable of accurately calculating EPC-induced PMMs in realistic materials is lacking.

Besides magnetic moments, phonons can also exhibit Hall effects [29–32] and topological characteristics, such as Berry curvature and Chern numbers [33–35]. When the time-reversal symmetry (TRS) is broken, phonon states with nonzero Chern numbers host a phonon analog of quantum anomalous Hall states, featuring topologically protected phonon edge currents. Nevertheless, TRS-breaking external fields for phonons, such as strong magnetic fields or Coriolis forces, often face experimental limitations [36, 37]. Consequently, phonon Chern states

driven by the phonon Zeeman splitting resulting from spin-phonon coupling (SPC) in magnets without requiring external fields are highly desirable. However, it is challenging to predict such intrinsic topological phonon states in magnets due to the inability to perform *ab initio* calculations of TRS-breaking phonon spectra [38–43].

To resolve these challenges, we establish an *ab initio* theory for determining EPC-induced magnetic properties of phonons, which enables first-principles calculations of previously inaccessible TRS-breaking phonon spectra across material classes from insulators to metals. Based on this theory, we demonstrate that EPC-induced PMMs can lead to large phonon Zeeman splittings through SPC in magnetic metals, which are orders of magnitude stronger than classical predictions from point-charge models [Fig. 1(a)]. Considering that these splittings could open significant topological gaps in phonon dispersions [Fig. 1(b)], we propose an inertially decoupled lattice model to realize intrinsic phonon Chern states in realistic materials. Furthermore, through first-principles calculations, we predict a family of promising candidate materials exhibiting intrinsic phonon Chern states. Our work establishes an *ab initio* theoretical foundation for investigating EPC-induced magnetic properties of phonons, which paves the way for further developments of phonon physics.

Ab initio theory for phonon Zeeman energy and phonon magnetic moment. Previous theories regarding magnetic properties of phonons driven by EPC have mainly been

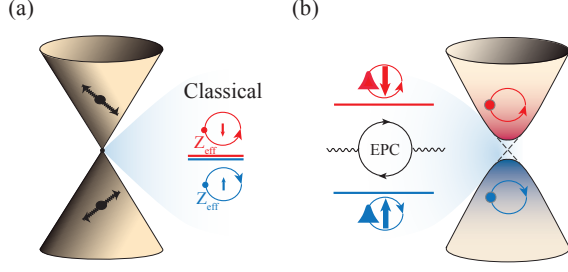


FIG. 1. Schematic of the phonon Zeeman splitting driven by (a) the classical PMM and (b) the EPC-enhanced PMM. In (a), the phonon band crossing point consists of two degenerate phonon modes vibrating in two different directions (black arrows), which can be recombined into left-circularly (red) and right-circularly (blue) polarized chiral phonons. The classical phonon Zeeman splitting deduced from the point-charge model (Z_{eff} is the effective charge) is negligible as a result of the significant atomic mass, whereas the EPC-induced phonon Zeeman splitting (b) is orders of magnitude larger. This significant splitting can open a substantial topologically nontrivial phonon gap, giving rise to the phonon Chern state with topological edge states [dashed lines in (b)].

applicable to insulators or semimetals, and are restricted to the Γ point [8, 11, 13, 15]. Since EPC is typically much more significant in metallic systems, we develop an *ab initio* theory that can generally calculate EPC-induced magnetic properties of phonons across the whole Brillouin zone for both metals and insulators, which is also compatible with previous theories [see the supplemental material (SM) [44]]. We will demonstrate our theory as follows.

Instead of directly calculating the magnetic moment of a single phonon, we focus on experimentally observable phonon Zeeman energy induced by the coupling between PMM and spins of electrons. We start from the total phonon Hamiltonian including the TRS-breaking perturbation as

$$H = \sum_{l,a} \frac{1}{2} p_{l,a}^2 + \frac{1}{2} \sum_{l,ab} D_{l,ab} u_{l,a} u_{l,b} - \sum_{l,ab} \eta_{l,ab} p_{l,a} u_{l,b}, \quad (1)$$

where $a, b = x, y, z$ represent the Cartesian coordinates, $l = 1, 2, \dots, N$ denotes the lattice site for a system containing N atoms, and $u_{l,a} = \sqrt{m} x_{l,a}$ represents the renormalized atomic displacement with m being the atomic mass. The last term in Eq. (1), denoted as δH , describes the TRS-breaking perturbation resulting from SPC [1], and $\eta_{l,ab}$ is a 3×3 real antisymmetric matrix satisfying $\eta_{l,ab} = -\eta_{l,ba}$. In addition, $p_{l,a} = \dot{u}_{l,a} + \sum_{l,b} \eta_{l,ab} u_{l,b}$ represents the canonical momentum [44]. By identifying the phonon angular momentum as $s_{l,c}^{\text{ph}} = \sum_{ab} \epsilon_{abc} u_{l,a} p_{l,b}$ (c is the direction of angular momentum), with ϵ_{abc} being the third-order Levi-Civita tensor, we can express δH as phonon Zeeman energy in a compact form

$E_Z = \boldsymbol{\eta} \cdot \mathbf{s}^{\text{ph}} = \sum_{l,ab} \eta_{l,c} s_{l,c}^{\text{ph}}$, where we have defined $\eta_{l,c} = \frac{1}{2} \sum_{ab} \epsilon_{abc} \eta_{l,ab}$. Notably, we find that the angular momentum of chiral phonon can be treated as an effective perturbative field to the electron-phonon coupled system, and thus the Zeeman energy of chiral phonon can be effectively regarded as a linear response.

Importantly, we will show that $\boldsymbol{\eta}$ can be derived from the TRS-breaking self-energy correction of chiral phonons. Within the framework of linear response theory, $\boldsymbol{\eta}$ is concisely expressed as $\boldsymbol{\eta}(\mathbf{q}, \omega) = \frac{1}{i\omega} \boldsymbol{\chi}^-(\mathbf{q}, \omega)$, where $\chi_c^-(\mathbf{q}, \omega) = \chi_{c,\uparrow}(\mathbf{q}, \omega) - \chi_{c,\downarrow}(\mathbf{q}, \omega)$ [see SM [44]], indicating that the spin polarization of electrons leads to Zeeman splittings of chiral phonons. The susceptibility $\chi_{c,s}(\mathbf{q}, \omega)$ for $s = \uparrow, \downarrow$ can be obtained through the Feynman diagram illustrated in Fig. 1(b),

$$\chi_{c,s}(\mathbf{q}, \omega) = \frac{2i\omega}{\hbar N_{\mathbf{k}}} \sum_{\mathbf{k}, \alpha\beta} |V_{c,s}^{\mathbf{k}, \alpha\beta}(\mathbf{q}, \omega)|^2 \frac{f(\epsilon_s^{\mathbf{k}+\mathbf{q}, \alpha}) - f(\epsilon_s^{\mathbf{k}, \beta})}{\hbar\omega - (\epsilon_s^{\mathbf{k}+\mathbf{q}, \alpha} - \epsilon_s^{\mathbf{k}, \beta})}. \quad (2)$$

Here, \mathbf{k} and \mathbf{q} represent the wave vectors of the electron and phonon, respectively, and ω is the phonon frequency. $N_{\mathbf{k}}$ is the total number of \mathbf{k} , and $\epsilon_s^{\mathbf{k}, \alpha}$ denotes the electronic band structure with band indices α . f is the Fermi-Dirac distribution, and $V_{c,s}^{\mathbf{k}, \alpha\beta}(\mathbf{q}, \omega)$ is the EPC tensor [45, 46]. It should be emphasized that all parameters in Eq. (2) can be directly obtained from first-principles calculations, without empirical inputs or additional assumptions. A non-zero $\boldsymbol{\chi}^-$ requires spin-polarized electronic states, for example, in ferromagnets. To realize large $\boldsymbol{\chi}^-$, there are two key points according to Eq. (2): (i) The contribution of EPC tensor $V_{c,s}^{\mathbf{k}, \alpha\beta}(\mathbf{q}, \omega)$ is substantial, and materials composed of light atoms tend to possess strong $V_{c,s}^{\mathbf{k}, \alpha\beta}(\mathbf{q}, \omega)$. (ii) When the energy difference $(\epsilon_s^{\mathbf{k}+\mathbf{q}, \alpha} - \epsilon_s^{\mathbf{k}, \beta})$ approaches $\hbar\omega$, it leads to an enhancement of $\boldsymbol{\chi}^-$. Consequently, we can conclude that EPC-induced large phonon Zeeman splittings are most likely to occur in ferromagnetic narrow-gap semiconductors, semimetals and metals containing light elements.

Then, PMM can be derived from the above phonon Zeeman energy as (see SM [44])

$$\mu_c^{\text{ph}} = -\frac{\partial E_Z}{\partial B_c} = -g_c^{\text{ph}} \frac{\mu_B}{\hbar} s_c^{\text{ph}}. \quad (3)$$

Here, μ_B denotes the Bohr magneton of electron, B_c is the effective magnetic field, and $g_c^{\text{ph}} = \frac{\hbar}{2i\omega} \frac{\partial \chi_c^+}{\partial E_F} g_c^e$ represents the effective Landé g -factor of the chiral phonon (see SM [44]), where E_F is the Fermi energy and $\chi_c^+(\mathbf{q}, \omega) = \chi_{c,\uparrow}(\mathbf{q}, \omega) + \chi_{c,\downarrow}(\mathbf{q}, \omega)$. g_c^e is the g -factor along c direction of electrons involved in EPC. Equation (3) enables first-principles calculations of PMM. The dimensionless parameter $\frac{\hbar}{2i\omega} \frac{\partial \chi_c^+}{\partial E_F}$ acts as an amplification factor dominated by the EPC tensor $V_{c,s}^{\mathbf{k}, \alpha\beta}$ and density of electron states near the Fermi energy [Eq. (S22) in SM [44]], and it allows the g -factor of the chiral phonon to reach the order of g_c^e , leading to a large PMM. This enhancement

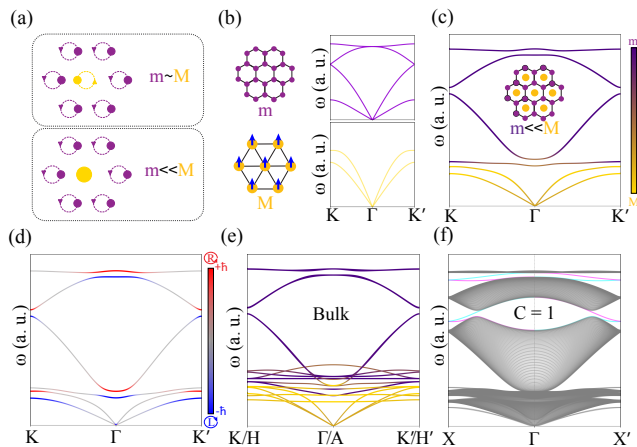


FIG. 2. Inertially decoupled model (IDM) and intrinsic phonon Chern states. (a) Schematic of chiral phonon modes in the high frequency regime: When $m \sim M$, both atoms contribute to high-frequency modes (upper panel); in the IDM condition ($m \ll M$), high-frequency modes are primarily contributed by light atoms (lower panel). (b) Phonon dispersions of nonmagnetic honeycomb lattice and ferromagnetic triangular lattice. (c-e) TRS-breaking phonon dispersions of the 2D IDM by combining the honeycomb and triangular lattices (c,d) and the 3D IDM by stacking 2D IDM along the z -direction (e). (f) Edge states (cyan/magenta) of the 2D IDM. Parameters are detailed in the SM [44].

of PMM originates from electron loop currents induced by the EPC-mediated angular momentum transfer from ions to electrons, where electron loop currents are significantly enhanced owing to the tiny electron mass. In contrast, within the classical framework, the phonon's g -factor is constrained to $10^{-5} \sim 10^{-4}$ order of g_c^e due to large ionic masses compared to the electron mass [11, 47].

Intrinsic phonon Chern states and the inertially decoupled model. The accurate calculation of phonon Zeeman splitting enables the determination of magnetic phonon spectra throughout the Brillouin zone, which is indispensable for exploring magnetic phonon topology. Following the analogy to the Chern state in the Haldane model [48], we adopt the two-dimensional (2D) honeycomb lattice [49–51] as an illustrative example. When either inversion symmetry (I) or TRS (T) is broken, each phonon Dirac cone at $K(K')$ valley acquires a finite gap, effectively gaining masses denoted as Δ_I and Δ_T , respectively. It has been shown that when $|\Delta_T| > |\Delta_I|$, band inversion occurs in one of the two Dirac cones, resulting in a topological phonon state with a Chern number of $|C| = 1$ [49].

However, it is challenging to realize such phonon Chern states in realistic materials with honeycomb lattices. Although Coriolis forces and strong magnetic fields can produce a nonzero Δ_T [49], these approaches either require large external fields or complex experimental measurements. In contrast, the phonon Zeeman splitting could

offer a sizable Δ_T in magnets without the need of external fields. To further satisfy the condition of $|\Delta_T| > |\Delta_I|$, it is necessary to minimize $|\Delta_I|$. Therefore, an elemental ferromagnetic honeycomb material inherently preserving inversion symmetry with $|\Delta_I| = 0$ would be the ideal candidate. Unfortunately, to our knowledge, no elemental ferromagnetic honeycomb material has been discovered. Furthermore, any honeycomb lattice composed of multiple elements could introduce a substantial Δ_I , which will make the condition $|\Delta_T| > |\Delta_I|$ difficult to satisfy.

To seek realistic materials that exhibit intrinsic phonon Chern states, we propose a practical composite lattice model, referred to as the inertially decoupled model that comprises two types of atoms with a significant mass (inertia) difference. A prototypical example of this model is constructed by combining a honeycomb lattice composed of nonmagnetic light atoms of mass m with a triangular lattice of heavy magnetic atoms of mass M ($m \ll M$), as shown in Figs. 2(b,c). Due to the difference in atomic inertia, the high-frequency and low-frequency dispersions are mainly contributed by the light and heavy atoms, respectively, as shown in Figs. 2(a,c), which is termed “inertially decoupled” (see SM [44] for details). Within the honeycomb sublattice, the inversion symmetry is preserved, resulting in a vanishing Δ_I mass at both the K and K' valleys. Meanwhile, the magnetic M atoms break TRS to generate large Zeeman splittings of chiral phonons via SPC, producing the desired large Δ_T mass. The large Δ_T opens a topologically nontrivial phonon gap (seen in Fig. 2(d)), thereby realizing an intrinsic phonon Chern state with $|C| = 1$, characterized by topologically protected edge states crossing the phonon gap, as shown in Fig. 2(f).

The inertially decoupled model is also applicable to three-dimensional (3D) magnets. Interestingly, when the nonmagnetic honeycomb lattice (the m sublayer) and the ferromagnetic triangular lattice (the M sublayer) are stacked alternately along the z -direction, each M sublayer effectively acts as a buffer layer that nearly decouples the phonon dispersions of adjacent m sublayers in the high-frequency regime. A representative phonon dispersion of such a 3D bulk model is shown in Fig. 2(e). Notably, since each m sublayer realizes a Chern state with $|C| = 1$, the system exhibits a 3D phonon Chern state. This configuration hosts multiple unidirectional phonon edge states resulting from a total Chern number $|C| = N_z$, where N_z is the number of m sublayers.

Candidate materials. Building upon our theory, we developed a dedicated computational module within Quantum ESPRESSO [52, 53] incorporating density-functional perturbation theory with Hubbard corrections (DFPT+U) [45, 46] for precise determination of response coefficients η and Landé g -factors of phonons. Then we add the effect of η into Schrödinger-like phonon equations constructed from the dynamical matrix through near-degenerate perturbation theory (see SM [44] for details),

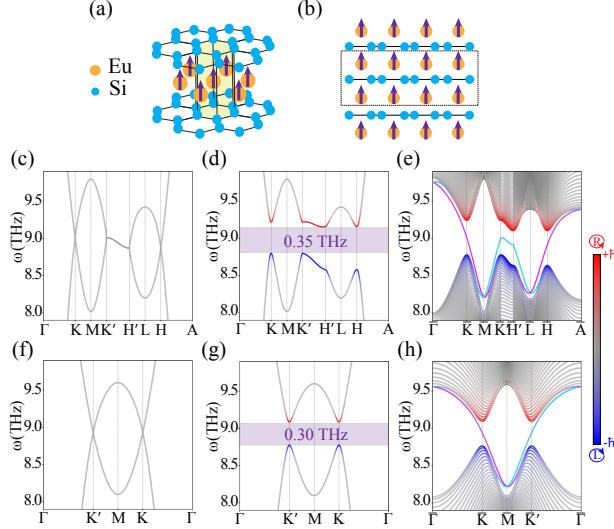


FIG. 3. Lattice structure and TRS-breaking phonon dispersions of ferromagnetic EuSi_2 . (a,b) The front view (a) and the side view (b) of the lattice structure of EuSi_2 . (c,d) The phonon dispersions of bulk EuSi_2 without (c) and with (d) the SPC, respectively. (e) The phonon dispersion of bulk EuSi_2 under open-boundary conditions. (f,g) The phonon dispersion of the sandwiched slab enclosed by the black rectangle in (b) without (f) and with (g) the SPC, respectively. (h) The phonon dispersion of the sandwiched slab under open-boundary conditions. The color gradient from red to blue represents the phonon angular momentum. Cyan and magenta colors in (c) and (h) label topological boundary modes residing on opposite boundaries.

yielding TRS-breaking phonon dispersions.

Through first-principles calculations guided by the inertially decoupled model, we identified five hexagonal ($P6/mmm$) magnets exhibiting intrinsic phonon Chern states, namely, EuSi_2 , GdSi_2 [59], EuGa_2 , GdGa_2 [60], and CrB_2 [61, 62]. Remarkably, they all have large observable topological phonon gaps at the K point defined as $\Delta_{\text{ph}} = \Delta_z - \gamma$, where $\Delta_z = 2|E_Z|$ is the phonon Zeeman splitting and γ is the phonon linewidth resulting from EPC [63, 64], as summarized in Table I. Note that the Zeeman splitting should be larger than the phonon linewidth to produce an observable phonon gap.

Here, we take EuSi_2 as a representative example (see SM [44] for details on all candidate materials). The lattice structures of EuSi_2 are illustrated in Figs. 3(a, b). Nonmagnetic Si atoms form a honeycomb-lattice layer, stacked alternately with a ferromagnetic Eu triangular-lattice layer, along the $[001]$ direction. The atomic masses of Si and Eu are approximately $28u$ and $152u$ (u is atomic mass unit), respectively, with each Eu atom carrying an out-of-plane magnetic moment of $7\mu_B$. As a result, EuSi_2 can be aptly described by our proposed inertially decoupled model.

Our first-principles calculations reveal that the EPC

induces a pronounced Zeeman splitting of chiral phonons in the high-frequency phonon dispersion of ferromagnetic EuSi_2 [see Figs. 3(c, d)], opening a sizable full topological gap (≈ 0.35 THz) throughout the Brillouin zone. Given that the Chern number remains $|C| = 1$ for all 2D k_z slices, EuSi_2 realizes a 3D layered phonon Chern state. This is further supported by the presence of boundary modes in the phonon dispersions of EuSi_2 under open-boundary conditions, as illustrated in Fig. 3(e). To achieve a 2D Chern state, we construct a dynamically-stable sandwiched slab featuring a Si sublayer between two Eu sublayers, as shown by the black rectangle in Fig. 3(b). By comparing Figs. 2(f) and 2(g), we can see that the phonon Zeeman splitting generates a substantial topologically nontrivial phonon gap (≈ 0.30 THz) with a Chern number of $|C| = 1$ featuring a pair of edge modes traversing the phonon gap, as shown in Fig. 3(h). This provides definitive evidence for intrinsic phonon Chern states.

TABLE I. The direct phonon gaps at K points for the candidate materials, where γ and Δ_z represent the phonon linewidth and the phonon Zeeman splitting, respectively. The observable phonon gap Δ_{ph} is defined as $\Delta_z - \gamma$.

Mat.	Δ_z (THz)	γ (THz)	Δ_{ph} (THz)
EuSi_2	0.426	0.049	0.377
GdSi_2	0.406	0.061	0.345
EuGa_2	0.134	0.028	0.106
GdGa_2	0.145	0.015	0.130
CrB_2	0.270	0.033	0.237

Discussion and conclusion. The intrinsic phonon Chern state, which hosts topologically protected edge phonon currents, holds significant potential for applications due to its operation without requiring strong external magnetic fields, Coriolis forces, or stress gradients [2, 49]. One potential advantage may be its ability to detect neutral particles by converting them into topological phonon edge currents. Neutral particles, especially dark matter particles, rarely participate in electromagnetic interactions, making their detection extremely challenging. However, if the energy transferred from the neutral particle to nucleus during the scattering or absorption falls within the first “conduction” band above the topological gap in the phonon dispersion, corresponding phonon modes can be excited [65, 66], driving the system out of equilibrium. As the system relaxes back to equilibrium, these high-frequency modes gradually shift to lower frequencies and necessarily cross the phonon Chern gap via topologically protected edge states, manifesting as a unidirectional edge phonon current immune to scattering [Fig. 4(a)]. This robust edge current is significantly more measurable than conventional delocalized bulk phonon excitations in materials. However, the operating temperature of detectors must be sufficiently low to pre-

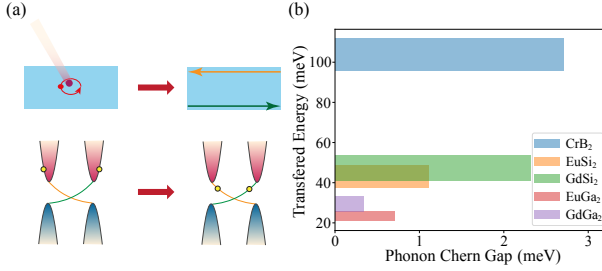


FIG. 4. Detection of neutral particles based on the intrinsic phonon Chern state. (a) Schematic illustrations of the detection process. Left: Neutral particles (red beam) excite phonon modes (yellow circles in the lower panel) in high-frequency bands. Right: These phonon modes gradually relax to lower-frequency regimes via topologically protected edge phonon channels (orange and green lines across the gap), generating robust unidirectional phonon edge currents (orange and green arrows). (b) Transferred energy ranges and phonon Chern gaps from proposed candidate materials [Tab. S2 in SM [44]].

vent thermal excitation from overcoming the phonon gap, which would otherwise disrupt these edge currents. Thus, a large phonon Chern gap is highly desired to elevate the working temperature. Figure 4(b) lists phonon Chern gaps and transferred energy ranges of proposed candidate materials (see SM [44] for details), with transferred energy spanning approximately 20 ~ 110 meV. This energy range corresponds to low-energy dark matter which recently attracts much attention, therefore our work provides a potential detection mechanism for this category of dark matter candidates [65, 66].

In summary, we have established an *ab initio* theory enabling systematic predictions of EPC-induced magnetic properties of phonons and TRS-breaking phonon dispersions for insulators, semimetals and metals. Based on our theory, we construct the inertially decoupled model to seek intrinsic phonon Chern states in realistic materials, and propose candidates exhibiting EPC-induced large topological phonon gaps exceeding 0.3 THz. Furthermore, we demonstrate the potential capability of these topological phonon states to detect neutral particles through robust phonon edge currents. These advances could open broad pathways for investigating phonon magnetic effects in quantum materials.

The authors thank Lei Zhang and Zuowei Liu for valuable discussions. This work is partly supported by National Key Projects for Research and Development of China (Grants No. 2024YFA1409100, No. 2021YFA1400400 and No. 2022YFA1403602), the Natural Science Foundation of Jiangsu Province (No. BK20220032, BK20233001, BK20243011), the Natural Science Foundation of China (No. 12074181, No. 12104217, No. 12174182, and No. 92365203), and the e-Science Center of Collaborative Innovation Center of Advanced Microstructures.

* zhanghj@nju.edu.cn; hqwang@nju.edu.cn

- [1] L. Zhang and Q. Niu, Angular Momentum of Phonons and the Einstein-de Haas Effect, *Phys. Rev. Lett.* **112**, 085503 (2014).
- [2] L. Zhang and Q. Niu, Chiral Phonons at High-Symmetry Points in Monolayer Hexagonal Lattices, *Phys. Rev. Lett.* **115**, 115502 (2015).
- [3] H. Zhu, J. Yi, M.-Y. Li, J. Xiao, L. Zhang, C.-W. Yang, R. A. Kaindl, L.-J. Li, Y. Wang, and X. Zhang, Observation of chiral phonons, *Science* **359**, 579 (2018).
- [4] H. Chen, W. Zhang, Q. Niu, and L. Zhang, Chiral phonons in two-dimensional materials, *2D Mater.* **6**, 012002 (2018).
- [5] D. M. Juraschek and N. A. Spaldin, Orbital magnetic moments of phonons, *Phys. Rev. Mater.* **3**, 064405 (2019).
- [6] H. Chen, W. Wu, J. Zhu, S. A. Yang, and L. Zhang, Propagating Chiral Phonons in Three-Dimensional Materials, *Nano Lett.* **21**, 3060 (2021).
- [7] D. M. Juraschek, T. Neuman, and P. Narang, Giant effective magnetic fields from optically driven chiral phonons in 4f paramagnets, *Phys. Rev. Res.* **4**, 013129 (2022).
- [8] Y. Ren, C. Xiao, D. Saparov, and Q. Niu, Phonon Magnetic Moment from Electronic Topological Magnetization, *Phys. Rev. Lett.* **127**, 186403 (2021).
- [9] D. Saparov, B. Xiong, Y. Ren, and Q. Niu, Lattice dynamics with molecular Berry curvature: Chiral optical phonons, *Phys. Rev. B* **105**, 064303 (2022).
- [10] T. Zhang and S. Murakami, Chiral phonons and pseudoangular momentum in nonsymmorphic systems, *Phys. Rev. Res.* **4**, L012024 (2022).
- [11] X.-W. Zhang, Y. Ren, C. Wang, T. Cao, and D. Xiao, Gate-Tunable Phonon Magnetic Moment in Bilayer Graphene, *Phys. Rev. Lett.* **130**, 226302 (2023).
- [12] J. Fransson, Chiral phonon induced spin polarization, *Phys. Rev. Res.* **5**, L022039 (2023).
- [13] J. Bonini, S. Ren, D. Vanderbilt, M. Stengel, C. E. Dreyer, and S. Coh, Frequency Splitting of Chiral Phonons from Broken Time-Reversal Symmetry in CrI₃, *Phys. Rev. Lett.* **130**, 086701 (2023).
- [14] S. Ren, J. Bonini, M. Stengel, C. E. Dreyer, and D. Vanderbilt, Adiabatic Dynamics of Coupled Spins and Phonons in Magnetic Insulators, *Phys. Rev. X* **14**, 011041 (2024).
- [15] W. Chen, X.-W. Zhang, Y. Su, T. Cao, D. Xiao, and S.-Z. Lin, Gauge theory of giant phonon magnetic moment in doped Dirac semimetals, *arXiv:2405.10318* (2024).
- [16] S. Chaudhary, D. M. Juraschek, M. Rodriguez-Vega, and G. A. Fiete, Giant effective magnetic moments of chiral phonons from orbit-lattice coupling, *Phys. Rev. B* **110**, 094401 (2024).
- [17] R. Merlin, Magnetophononics and the Chiral Phonon Misnomer, *arXiv:2404.19593* (2024).
- [18] R. Xue, Z. Qiao, Y. Gao, and Q. Niu, Extrinsic mechanisms of phonon magnetic moment, *arXiv:2501.03204* (2025).
- [19] B. Cheng, T. Schumann, Y. Wang, X. Zhang, D. Barbalas, S. Stemmer, and N. P. Armitage, A Large Effective Phonon Magnetic Moment in a Dirac Semimetal, *Nano Lett.* **20**, 5991 (2020).
- [20] S. R. Tauchert, M. Volkov, D. Ehberger, D. Kazenwadel, M. Evers, H. Lange, A. Donges, A. Book, W. Kreuz-

- paintner, U. Nowak, and P. Baum, Polarized phonons carry angular momentum in ultrafast demagnetization, *Nature* **602**, 73 (2022).
- [21] G. Xiong, H. Chen, D. Ma, and L. Zhang, Effective magnetic fields induced by chiral phonons, *Phys. Rev. B* **106**, 144302 (2022).
- [22] J. Luo, T. Lin, J. Zhang, X. Chen, E. R. Blackert, R. Xu, B. I. Yakobson, and H. Zhu, Large effective magnetic fields from chiral phonons in rare-earth halides, *Science* **382**, 698 (2023).
- [23] R. Nabi, J. K. Staab, A. Mattioni, J. G. C. Kragoskow, D. Reta, J. M. Skelton, and N. F. Chilton, Accurate and Efficient Spin-Phonon Coupling and Spin Dynamics Calculations for Molecular Solids, *J. Am. Chem. Soc.* **145**, 24558 (2023).
- [24] H. Ueda, M. García-Fernández, S. Agrestini, C. P. Romao, J. van den Brink, N. A. Spaldin, K.-J. Zhou, and U. Staub, Chiral phonons in quartz probed by X-rays, *Nature* **618**, 946 (2023).
- [25] F. G. G. Hernandez, A. Baydin, S. Chaudhary, F. Tay, I. Katayama, J. Takeda, H. Nojiri, A. K. Okazaki, P. H. O. Rappl, E. Abramof, M. Rodriguez-Vega, G. A. Fiete, and J. Kono, Chiral Phonons with Giant Magnetic Moments in a Topological Crystalline Insulator, *Sci. Adv.* **9**, eadj4074 (2023).
- [26] D. Lujan, J. Choe, S. Chaudhary, G. Ye, C. Nnokwe, M. Rodriguez-Vega, J. He, F. Y. Gao, T. N. Nunley, E. Baldini, J. Zhou, G. A. Fiete, R. He, and X. Li, Spin-orbit exciton-induced phonon chirality in a quantum magnet, *Proc. Natl. Acad. Sci. USA* **121**, e2304360121 (2024).
- [27] F. Wu, J. Zhou, S. Bao, L. Li, J. Wen, Y. Wan, and Q. Zhang, Magnetic switching of phonon angular momentum in a ferrimagnetic insulator, *arXiv:2501.10650* (2025).
- [28] C. S. Davies, F. G. N. Fennema, A. Tsukamoto, I. Razdolski, A. V. Kimel, and A. Kirilyuk, Phononic switching of magnetization by the ultrafast Barnett effect, *Nature* **628**, 540 (2024).
- [29] C. Strohm, G. L. J. A. Rikken, and P. Wyder, Phenomenological Evidence for the Phonon Hall Effect, *Phys. Rev. Lett.* **95**, 155901 (2005).
- [30] L. Sheng, D. N. Sheng, and C. S. Ting, Theory of the Phonon Hall Effect in Paramagnetic Dielectrics, *Phys. Rev. Lett.* **96**, 155901 (2006).
- [31] Y. Kagan and L. A. Maksimov, Anomalous Hall Effect for the Phonon Heat Conductivity in Paramagnetic Dielectrics, *Phys. Rev. Lett.* **100**, 145902 (2008).
- [32] K. Sun, Z. Gao, and J.-S. Wang, Current-induced phonon hall effect, *Phys. Rev. B* **102**, 134311 (2020).
- [33] L. Zhang, J. Ren, J.-S. Wang, and B. Li, Topological Nature of the Phonon Hall Effect, *Phys. Rev. Lett.* **105**, 225901 (2010).
- [34] T. Qin, J. Zhou, and J. Shi, Berry curvature and the phonon Hall effect, *Phys. Rev. B* **86**, 104305 (2012).
- [35] Y. Liu, Y. Xu, and W. Duan, Berry phase and topological effects of phonons, *Natl. Sci. Rev.* **5**, 314 (2017).
- [36] Y. Liu, C.-S. Lian, Y. Li, Y. Xu, and W. Duan, Pseudospins and Topological Effects of Phonons in a Kekulé Lattice, *Phys. Rev. Lett.* **119**, 255901 (2017).
- [37] S. Park and B.-J. Yang, Phonon Angular Momentum Hall Effect, *Nano Lett.* **20**, 7694 (2020).
- [38] R. Süssstrunk and S. D. Huber, Classification of topological phonons in linear mechanical metamaterials, *Proc. Natl. Acad. Sci. USA* **113**, E4767 (2016).
- [39] B. Peng, Y. Hu, S. Murakami, T. Zhang, and B. Monserrat, Topological phonons in oxide perovskites controlled by light, *Sci. Adv.* **6**, eabd1618 (2020).
- [40] J. Li, J. Liu, S. A. Baronett, M. Liu, L. Wang, R. Li, Y. Chen, D. Li, Q. Zhu, and X.-Q. Chen, Computation and data driven discovery of topological phononic materials, *Nat. Commun.* **12**, 1204 (2021).
- [41] Y. Xu, M. G. Vergniory, D.-S. Ma, J. L. Mañes, Z.-D. Song, B. A. Bernevig, N. Regnault, and L. Elcoro, Catalog of topological phonon materials, *Science* **384**, eadf8458 (2024).
- [42] R. Zhang, H. Sheng, J. Deng, Z. Fang, Z. Yang, and Z. Wang, Unconventional phonon spectra and obstructed edge phonon modes, *Sci. China: Phys., Mech. Astron.* **67**, 246811 (2023).
- [43] Z.-K. Ding, Y.-J. Zeng, W. Liu, L.-M. Tang, and K.-Q. Chen, Topological Phonons and Thermoelectric Conversion in Crystalline Materials, *Adv. Funct. Mater.* **34**, 2401684 (2024).
- [44] See the Supplemental Material, which includes Refs. [54–58], for additional information about the methods and additional data and discussion.
- [45] F. Giustino, Electron-phonon interactions from first principles, *Rev. Mod. Phys.* **89**, 015003 (2017).
- [46] J.-J. Zhou, J. Park, I. Timrov, A. Floris, M. Cococcioni, N. Marzari, and M. Bernardi, *Ab Initio* Electron-Phonon Interactions in Correlated Electron Systems, *Phys. Rev. Lett.* **127**, 126404 (2021).
- [47] Q. Wang, S. Li, J. Zhu, H. Chen, W. Wu, W. Gao, L. Zhang, and S. A. Yang, Chiral phonons in lattices with C_4 symmetry, *Phys. Rev. B* **105**, 104301 (2022).
- [48] F. D. M. Haldane, Model for a Quantum Hall Effect without Landau Levels: Condensed-Matter Realization of the “Parity Anomaly”, *Phys. Rev. Lett.* **61**, 2015 (1988).
- [49] Y. Liu, Y. Xu, S.-C. Zhang, and W. Duan, Model for topological phononics and phonon diode, *Phys. Rev. B* **96**, 064106 (2017).
- [50] N. Bonini, M. Lazzeri, N. Marzari, and F. Mauri, Phonon Anharmonicities in Graphite and Graphene, *Phys. Rev. Lett.* **99**, 176802 (2007).
- [51] J. Li, J. Li, J. Tang, Z. Tao, S. Xue, J. Liu, H. Peng, X.-Q. Chen, J. Guo, and X. Zhu, Direct Observation of Topological Phonons in Graphene, *Phys. Rev. Lett.* **131**, 116602 (2023).
- [52] P. Giannozzi, S. Baroni, N. Bonini, M. Calandra, R. Car, C. Cavazzoni, D. Ceresoli, G. L. Chiarotti, M. Cococcioni, I. Dabo, A. Dal Corso, S. De Gironcoli, S. Fabris, G. Fratesi, R. Gebauer, U. Gerstmann, C. Gougoussis, A. Kokalj, M. Lazzeri, L. Martin-Samos, N. Marzari, F. Mauri, R. Mazzarello, S. Paolini, A. Pasquarello, L. Paulatto, C. Sbraccia, S. Scandolo, G. Sclauzero, A. P. Seitsonen, A. Smogunov, P. Umari, and R. M. Wentzcovitch, QUANTUM ESPRESSO: A modular and open-source software project for quantum simulations of materials, *J. Phys.: Condens. Matter* **21**, 395502 (2009).
- [53] P. Giannozzi, O. Andreussi, T. Brumme, O. Bunau, M. Buongiorno Nardelli, M. Calandra, R. Car, C. Cavazzoni, D. Ceresoli, M. Cococcioni, N. Colonna, I. Carnimeo, A. Dal Corso, S. De Gironcoli, P. Delugas, R. A. DiStasio, A. Ferretti, A. Floris, G. Fratesi, G. Fugallo, R. Gebauer, U. Gerstmann, F. Giustino, T. Gorni, J. Jia, M. Kawamura, H.-Y. Ko, A. Kokalj, E. Küçükbenli, M. Lazzeri, M. Marsili, N. Marzari, F. Mauri, N. L.

- Nguyen, H.-V. Nguyen, A. Otero-de-la Roza, L. Paulatto, S. Ponc  , D. Rocca, R. Sabatini, B. Santra, M. Schlipf, A. P. Seitsonen, A. Smogunov, I. Timrov, T. Thonhauser, P. Umari, N. Vast, X. Wu, and S. Baroni, Advanced capabilities for materials modelling with Quantum ESPRESSO, *J. Phys.: Condens. Matter* **29**, 465901 (2017).
- [54] S. Baroni, S. de Gironcoli, A. Dal Corso, and P. Giannozzi, Phonons and related crystal properties from density-functional perturbation theory, *Rev. Mod. Phys.* **73**, 515 (2001).
- [55] L. Zhang, H. Wang, M. C. Muniz, A. Z. Panagiotopoulos, R. Car, and W. E, A deep potential model with long-range electrostatic interactions, *J. Chem. Phys.* **156**, 124107 (2022).
- [56] A. Togo, L. Chaput, T. Tadano, and I. Tanaka, Implementation strategies in phonopy and phono3py, *J. Phys.: Condens. Matter* **35**, 353001 (2023).
- [57] A. Togo, First-principles Phonon Calculations with Phonopy and Phono3py, *J. Phys. Soc. Jpn.* **92**, 012001 (2023).
- [58] T. Fukui, Y. Hatsugai, and H. Suzuki, Chern Numbers in Discretized Brillouin Zone: Efficient Method of Computing (Spin) Hall Conductances, *J. Phys. Soc. Jpn* **74**, 1674 (2005).
- [59] I. Mayer, E. Yanir, and I. Shidlovsky, Dimorphism of rare earth disilicides, *Inorg. Chem.* **6**, 842 (1967).
- [60] J. Barandiaran, D. Gignoux, and J. Rodriguez-Fernandez, Magnetic properties and magnetic structure of hexagonal GdGa₂ and GdCu₅ compounds, *Phys. B* **154**, 293 (1989).
- [61] G. E. Grechnev, A. S. Panfilov, A. V. Fedorchenko, V. B. Filippov, A. B. Lyashchenko, and A. N. Vasiliev, Effect of pressure on the magnetic properties of CrB₂, *Low Temp. Phys.* **35**, 531 (2009).
- [62] A. Bauer, A. Regnat, C. G. F. Blum, S. Gottlieb-Sch  nmeyer, B. Pedersen, M. Meven, S. Wurmehl, J. Kune  , and C. Pfleiderer, Low-temperature properties of single-crystal CrB₂, *Phys. Rev. B* **90**, 064414 (2014).
- [63] A. Debernardi, Phonon linewidth in III-V semiconductors from density-functional perturbation theory, *Phys. Rev. B* **57**, 12847 (1998).
- [64] X. Tang and B. Fultz, First-principles study of phonon linewidths in noble metals, *Phys. Rev. B* **84**, 054303 (2011).
- [65] Y. Kahn, G. Krnjaic, and B. Mandava, Dark Matter Detection with Bound Nuclear Targets: The Poisson Phonon Tail, *Phys. Rev. Lett.* **127**, 081804 (2021).
- [66] C. P. Romao, R. Catena, N. A. Spaldin, and M. Matas, Chiral phonons as dark matter detectors, *Phys. Rev. Res.* **5**, 043262 (2023).